Nanotechnology **20** (2009) 425101 (9pp) doi:10.1088/0957-4484/20/42/425101

Nanomechanical properties of vimentin intermediate filament dimers

Zhao Qin[1,2], **Laurent Kreplak**[3] **and Markus J Buehler**[1,2,4,5]

[1] Laboratory for Atomistic and Molecular Mechanics, Department of Civil and Environmental Engineering, Massachusetts Institute of Technology, 77 Massachusetts Avenue, Room 1-235A&B, Cambridge, MA 02139, USA
[2] Center for Materials Science and Engineering, Massachusetts Institute of Technology, 77 Massachusetts Avenue, Cambridge, MA 02139, USA
[3] Department of Physics and Atmospheric Science, Dalhousie University, Halifax, NS, B3H 3J5, Canada
[4] Center for Computational Engineering, Massachusetts Institute of Technology, 77 Massachusetts Avenue, Cambridge, MA 02139, USA

E-mail: mbuehler@MIT.EDU

Received 3 July 2009, in final form 7 August 2009
Published 25 September 2009
Online at stacks.iop.org/Nano/20/425101

Abstract
The cell's cytoskeleton, providing the cell with structure and shape, consists of a complex array of structural proteins, including microtubules, microfilaments and intermediate filaments. Intermediate filaments play a crucial role in mechanotransduction and in providing mechanical stability to cells, in particular under large deformation. By utilizing molecular simulation, here we report a nanomechanical analysis of vimentin intermediate filament dimers, the basic building blocks of intermediate filaments. We describe a detailed analysis of the mechanical properties and associated deformation mechanisms, and find that mechanical stretch induces a transition from alpha-helices to beta-sheets, a phenomenon known as alpha–beta transition. A comparison of the Young's modulus predicted from simulation with experimental measurements is provided, and good agreement is found. We present an analysis of structural changes during deformation, domain unfolding patterns, rate dependence of the rupture force and associated changes in the energy landscape, and conclude with a discussion of potential implications for mechanobiology and the development of *de novo* protein materials.

(Some figures in this article are in colour only in the electronic version)

1. Introduction

Intermediate filaments (often abbreviated as IFs), in addition to microtubules and microfilaments, are one of the three major components of the cytoskeleton in eukaryotic cells [1–4]. Intermediate filaments are crucial in defining key mechanical functions of cells such as cell migration, cell division and mechanotransduction, and have also been referred to as the 'safety belts of cells' as they play a role in preventing exceedingly large cell stretch [5–8]. Vimentin is a specific type of this protein filament found in fibroblasts, leukocytes and blood vessel endothelial cells, representing the most widely distributed type of intermediate filaments. Earlier studies focused on analyzing the mechanical signature of intermediate filaments have suggested that they are highly sensitive to applied forces at small levels, while they can sustain extremely large deformations of up to 300% under tension [4, 9, 10]. It has also been observed that, due to severe stiffening, the tangent modulus of intermediate filaments increases many times during deformation, a property that is believed to be crucial for providing mechanical stability to cells at large stretch.

Intermediate filaments form hierarchical structures as shown in figure 1, ranging from dimers, tetramers, unit length filaments and full-length filaments to the cellular scale. The intermediate filament dimer represents the most fundamental building block, which contains 466 amino acid residues. Each dimer consists of four major structural segments linked in series in the sequence 1A (residues 78–138), 1B (residues 147–247), 2A (residues 264–283) and 2B (residues 291–405),

[5] Author to whom any correspondence should be addressed.

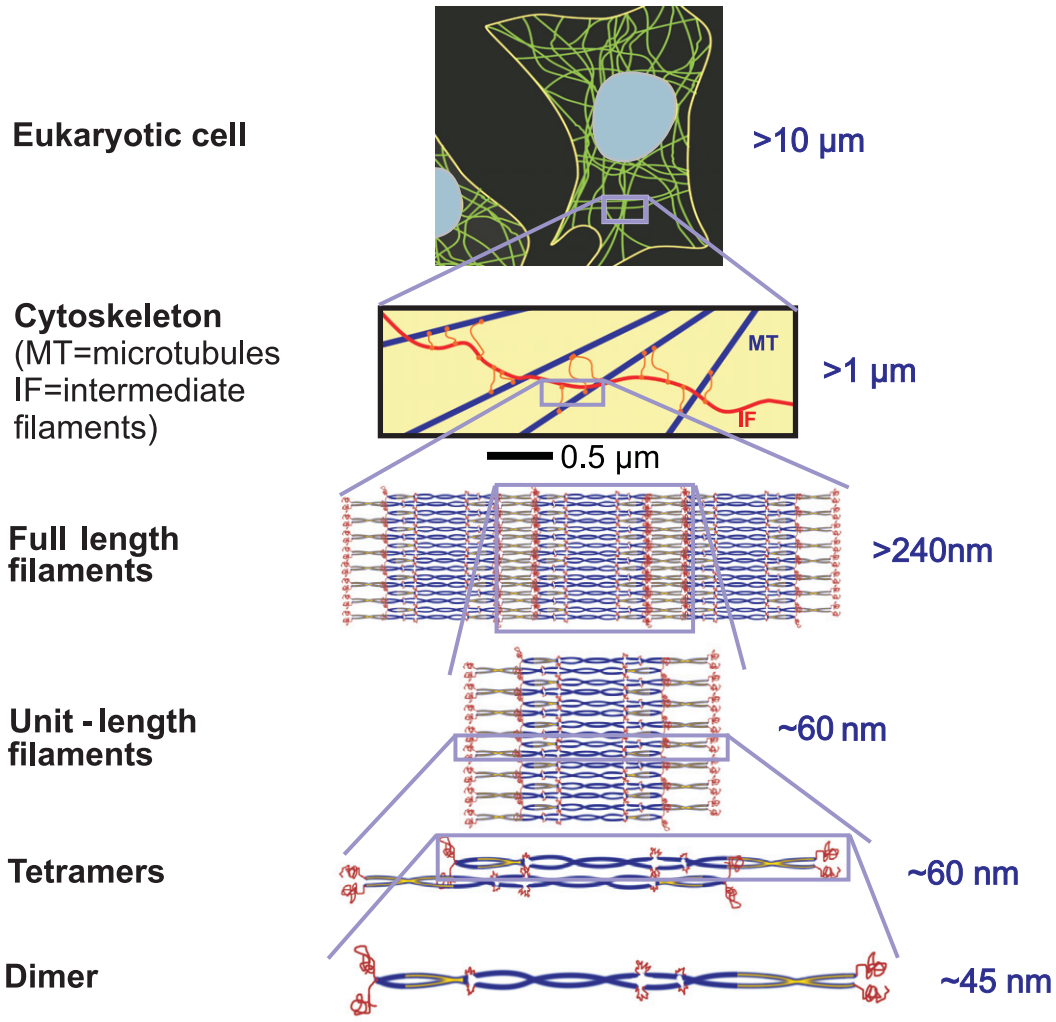

Figure 1. The hierarchical structure of intermediate filaments, from atomic to cellular scales. The focus of the present study is the dimer structure, the basic building block of intermediate filaments.

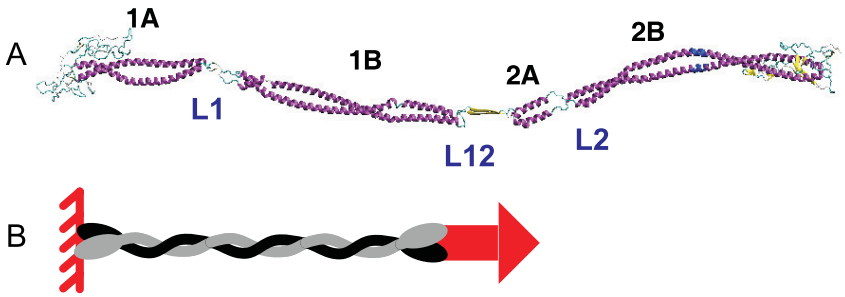

Figure 2. Molecular structure of the vimentin dimer and loading condition used in this study. Panel A: schematic geometry of the dimer geometry, including labels identifying the various segments and linker domains (the overall length of the dimer filament is ≈49 nm). Panel B: schematic of the pulling geometry and implementation of mechanical tensile test. The end of the dimer is fixed on the left and the protein is pulled at the right end at a constant pulling velocity, v.

connected by linkers L1, L12 and L2 (figure 2(A)). The four structural segments are alpha-helical proteins, whereas the linker domains are either unstructured or feature a beta-sheet secondary structure. Although there exists clear evidence that intermediate filaments play a key role in important physiological and pathological mechanisms, a molecular-level nanomechanical analysis of this protein structure remains elusive. Earlier molecular dynamics studies have focused solely on a small section of the 1A and 2B domain [11, 12], without considering the properties of the whole dimer structure as shown in figure 2(A). Furthermore, recent experimental studies using atomic force microscopy (AFM) analysis focused on the mechanical properties of entire filaments [10, 13]. However, the details of the underlying molecular mechanisms

of deformation remain unknown, and no analysis has been reported at the level of individual dimers. Here we carry out a series of systematic molecular dynamics simulations to probe the response of entire intermediate filament dimers to mechanical tensile stretch, using tensile loading boundary conditions as shown in figure 2(B). Specifically, the aim of our investigations is to elucidate the basis for their great extensibility and stiffening properties, as well as associated molecular deformation and domain unfolding mechanisms of the most fundamental building block of this protein.

2. Results

We study the nanomechanical properties of the vimentin intermediate filament dimer structure by carrying out an engineering tensile test as schematically shown in figure 2(B) (for details of computational methods see section 4). The dimer structure is stretched until all helical domains are fully extended. Figure 3(A) shows two characteristic force–strain curves for two pulling speeds (0.01 and 0.1 Å ps^{-1}). The simulations reveal three distinct regimes of deformation. In the first regime (I), the pulling force increases linearly with strain until it reaches an angular point, where a dramatic change in the slope emerges (the angular point corresponds to the point where the first unfolding in the protein occurs). In regime (I), the structure is under elastic deformation, where the force increases linearly with strain. This type of elastic deformation of the coiled-coil structure has also been observed experimentally [14]. In the second regime (II), the force–strain curve resembles a plateau, where the pulling force remains almost constant with a slight increase of force at increasing deformation. It is found that unfolding of all alpha-helical domains occurs in this regime. In the third regime (III), the stretching force increases rapidly as the strain increases, indicating a significant stiffening of the local (tangent) elastic properties. This is caused by pulling the unfolded polypeptide backbone of the protein, where the stretching of covalent bonds leads to a much increased stiffness. The overall characteristics of the force–strain curves of the dimer share similarities with stretching of individual alpha-helices [11, 15] as well as with myosin coiled-coil structures [16], which agrees with the fact that most parts of the vimentin dimer are composed of coiled coils (as shown in figure 2(B)). Regime (II) represents the main unfolding regime, where the average force in this regime approximates the protein's unfolding force. The slight increase of the force in this regime (approximately 1.079 pN per % strain, as shown in figure 3(A)) is due to the fact that, as more turns in the alpha-helical protein are unfolded, a larger rupture force is required since the failure probability is decreased for a smaller number of remaining turns [17]. It is noted that in experimental and simulation studies of the myosin coiled-coil protein, the strain–force curve shows a very similar behavior and the same level of unfolding force [18] (a detailed comparison will be presented below).

Calculation of the Young's modulus for small deformation (calculated in the pre-angular point regime (I) shown in figure 3(A), where the dimer is deformed homogeneously

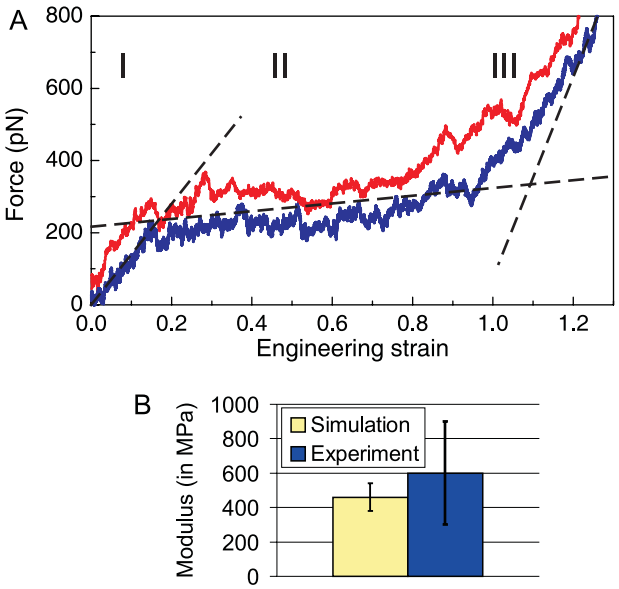

Figure 3. Mechanical analysis of the vimentin intermediate filament dimer under tensile deformation. Panel A: force–strain relations for tensile deformation of the vimentin dimer (0.01 Å s^{-1} (blue) and 0.1 Å ps^{-1} (red) pulling speeds). The force–strain curve features three regimes: (I) the force increases linearly with strain until the rupture of the H-bonds and uncoiling of alpha-helices sets in (in agreement with recent theoretical studies [17] and experimental results [18]). (II) A plateau of a constant force is found during which the unfolding process takes place. (III) The filament stiffens significantly due to stretching of the protein backbone. The figure clearly illustrates the characteristic softening–stiffening behavior associated with intermediate filaments. The intersection of the fits to regimes (I) and (II) denotes the angular point. Panel B: small-deformation Young's modulus, comparing simulation and experimental results.

before unfolding sets in) leads to values in the range of 380–540 MPa. This is in close agreement with experimental results from corresponding vimentin intermediate filament bending experiments, which show moduli in the range of 300–900 MPa [19]. This agreement supports the notion that intermediate filaments should be considered as a continuous body in the very-small-deformation regime where no unfolding or sliding occurs between individual dimers. A comparison between simulation and experiment is provided in figure 3(B).

Our simulations enable us to carry out a detailed mechanistic and structural analysis of deformation mechanisms. We begin by analyzing cartoon visualizations of the filament structures at different levels of applied strain. Figure 4 displays snapshots of the structural deformation during the stretching simulation of the dimer. Once tensile load is applied, the four segments align in the pulling direction and the coiled-coil protein domains are stretched slightly to mediate the elongation. No rupture or domain unfolding is observed until the applied strain is larger than 12%, where the 2A segment begins to uncoil first (this refers to deformation in regime (I)). We observe that the uncoiling of alpha-helical structures occurs simultaneously with the formation of beta-sheet protein domains, a phenomenon referred to as α–β transition. The pulling force causes the two uncoiled chains to come sufficiently close to

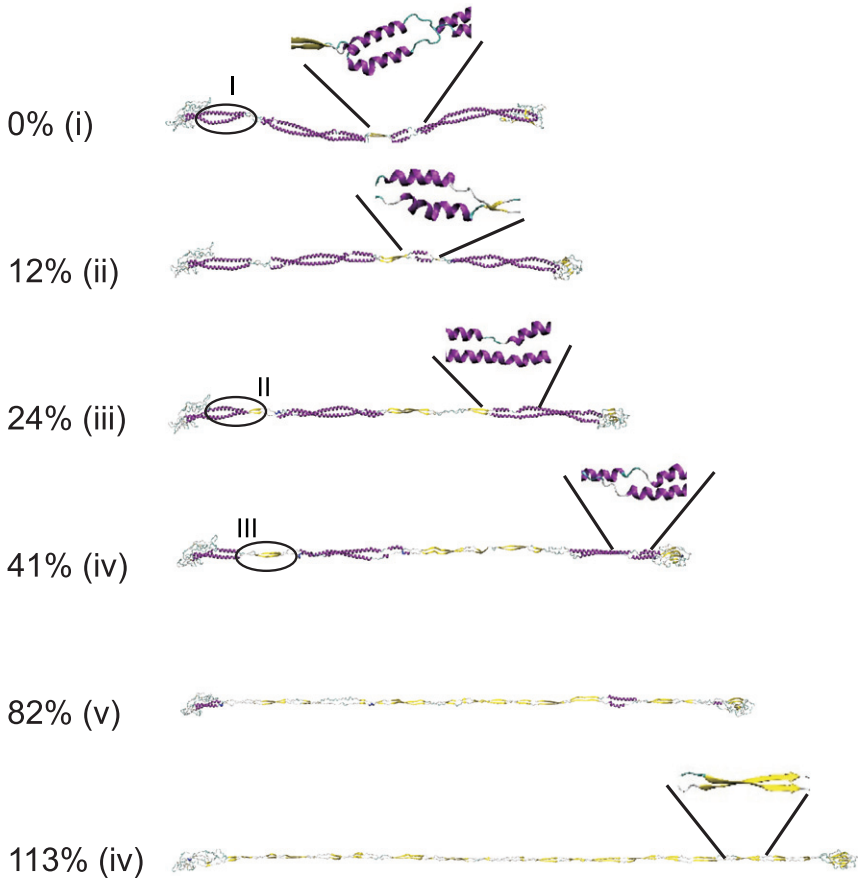

Figure 4. Simulation snapshots during pulling of the dimer. As the strain is increased, the structure loses its alpha-helical-dominated structure and beta-sheet domains are formed. The inlays show detailed views of the molecular structure at various levels of strain.

form a beta-sheet protein domain. We show details of the structural transition of the full dimer during the stretching process in figure 5(A). This plot depicts the structural character of each amino acid, plotted over the amino acid number and the corresponding level of strain. Figure 5(B) shows atomistic-level details of the α–β transition process, illustrating the mechanisms by which beta-sheets are formed due to uncoiling of pairs of alpha-helical domains (results shown for the right part of the 1A segment). The α–β transition seen here has also been observed in experimental studies, where it was shown that the secondary structure of double-stranded coiled-coil proteins gradually transforms into beta-sheets under applied tensile load [14, 20–22].

Further structural analysis is shown in figure 6, where we plot the number of amino acids associated with alpha-helical and beta-sheet secondary structures as a function of the applied tensile strain in a geometry–strain map. The results shown in figure 6 confirm that the number of amino acids in the alpha-helical state is approximately constant for strains smaller than 12%, which demonstrates that the structure remains intact. The reason why the 2A segment ruptures first is that, while the other three segments are coiled coils, the 2A segment is essentially a parallel alpha-helical bundle, which has a lower mechanical stability against tensile stretch as pointed out in earlier work [23, 24]. Once the 2A segment is fully uncoiled at $\approx$20% strain, the other segments 1B, 1A and 2B begin to uncoil sequentially. The geometry–strain map shown in figure 6(A) (upper part) confirms that the segments do not unfold simultaneously, but rather in a sequential process. The unfolding sequence is indicated in figure 6(B). This sequence is highly repeatable at different pulling velocities. The number of amino acids associated with alpha-helices decreases from $\approx$520 to zero between 12% and 110% strain. Simultaneously, the number of beta-sheet-associated amino acids increases from $\approx$10 to $\approx$370, supporting the notion that most amino acids in the dimer structure turn from alpha-helical dominant structures to beta-sheet structures under large deformation (in agreement with the visualizations shown in figure 4). It is noted that the $\approx$10 beta-sheet-associated amino acids in the beginning (at zero deformation) correspond to the short beta-strand found in the L12 linker. Table 1 shows a summary of the domain unfolding pattern properties and the dependence on the applied strain for different pulling velocities. The comparison of the unfolding dynamics at different pulling velocities confirms that the sequence remains identical and is highly repeatable.

We provide further analysis of the structural changes as strain is increased by carrying out a radial distribution function (RDF) analysis. The RDF analysis can elucidate if the system is in the solid state and gives the character of atomistic structure. Figure 7 shows the RDF for our dimer structure at pulling strain varies from 0 to 120% strain. The first

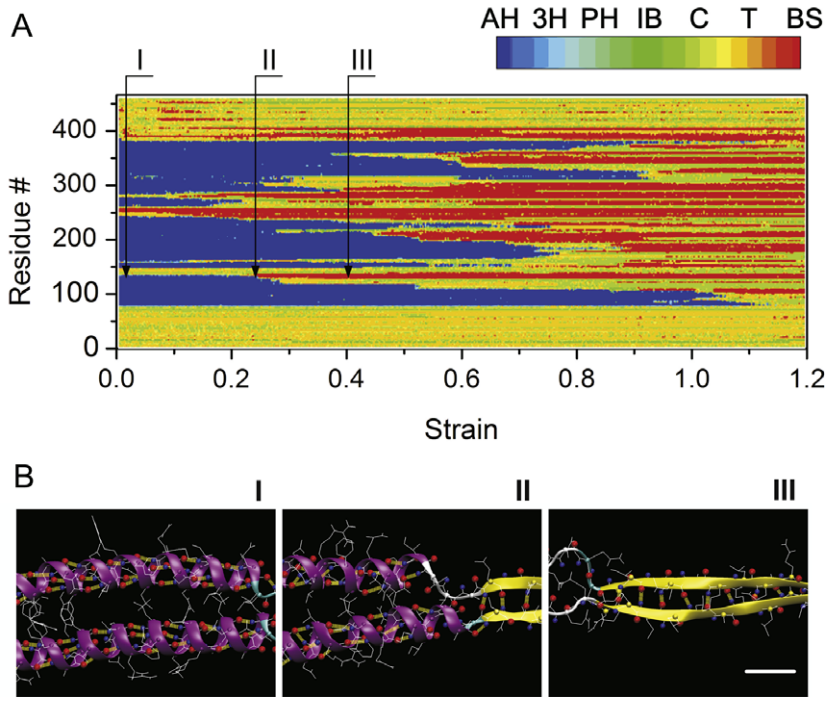

Figure 5. Detailed view of the atomistic and molecular processes during the alpha–beta transition under stretching of the intermediate filament dimer. Panel A: the spectrum of the structural transition at 0.01 Å ps^{-1} pulling speed. The plot shows the structural character of each amino acid of a monomer (with 466 amino acids in total) in the vimentin dimer during the entire stretching process. (Since the other monomer shows a symmetric behavior, it is not shown here.) The color bar indicating the structural character is separated into seven parts and corresponds to α-helix (AH), 3–10 helix (3H), phi-helix (PH), isolated-bridge (IB), coil (C), turn (T) and β-sheet (BS). Panel B: the snapshots show the structural detail of the right part of the 1A region (residues 114–138) that correspond to those views highlighted in figure 4 and regions pointed out in panel A. The scale bar is 5 Å. Hydrogen bonds are shown by yellow dashed lines, and in subfigure I they have an average value of 2 Å (O–H distance) in the convolution part, while in subfigure II it is measured to be 2.36 Å.

Table 1. Summary of domain unfolding pattern and structural parameters of domains (for geometry see figure 2(A)). The comparison of the unfolding dynamics at different pulling velocities confirms that the sequence remains identical and is highly repeatable.

	Strain at beginning of unfolding			Strain at end of unfolding			Unfolding strain $\Delta\varepsilon$			
Pulling speed (in Å ps^{-1})										
Segment	0.01	0.05	0.1	0.01	0.05	0.1	0.01	0.05	0.1	Length of segment (nm)
2A	12%	8%	9%	20%	24%	21%	8%	16%	12%	2
1B	22%	23%	18%	84%	104%	90%	62%	81%	72%	14
1A	25%	28%	20%	108%	118%	112%	83%	90%	92%	8
2B	30%	32%	27%	102%	104%	106%	72%	72%	79%	16

peak at 3.84 Å, relates to the nearest distance between alpha carbons in the backbone and shows the common structural character of the protein material. The other peaks at 5.00, 5.46, 6.20 and 8.70 Å indicate the second-, third-, fourth-and fifth-neighbor structure of the protein system, providing detailed information about the secondary and higher level structures. At zero deformation, these peaks show the characteristic pattern of an alpha-helical-rich material. During increasing strain, the higher-order peaks (other than the first peak) become less obvious and broader, revealing the characteristics of structural changes as the protein undergoes tensile deformation. The density distribution becomes broader, reflecting the loss of the alpha-helix-dominated structure in the rod-like domain. As the strain is increased, peaks at distances of 4.7, 6.0 and 7.0 Å emerge (see figure 7(B)), featuring the signature of beta-sheet-rich domains. This indicates that the structure has rearranged from an alpha-helical structure to a beta-sheet structure, in agreement with the results shown in figure 6 and the visual analysis shown in figure 4.

We extend the mechanical analysis by performing stretching simulations with pulling rates ranging from 0.0001 to 1 Å ps^{-1}. The unfolding force at the angular point (denoting the onset of domain unfolding in the protein) is plotted as a function of the pulling speed in figure 8(A). The results show a significant dependence of the unfolding force as a function of pulling velocity, reaching a plateau value for small pulling speeds of the order of ≈100 pN. The parameters in the Bell model are fitted according to the MD simulation results for the dimer shown in figure 8(A). We obtain for the slow deformation regime, $E_b = 14.05$ kcal mol^{-1} and

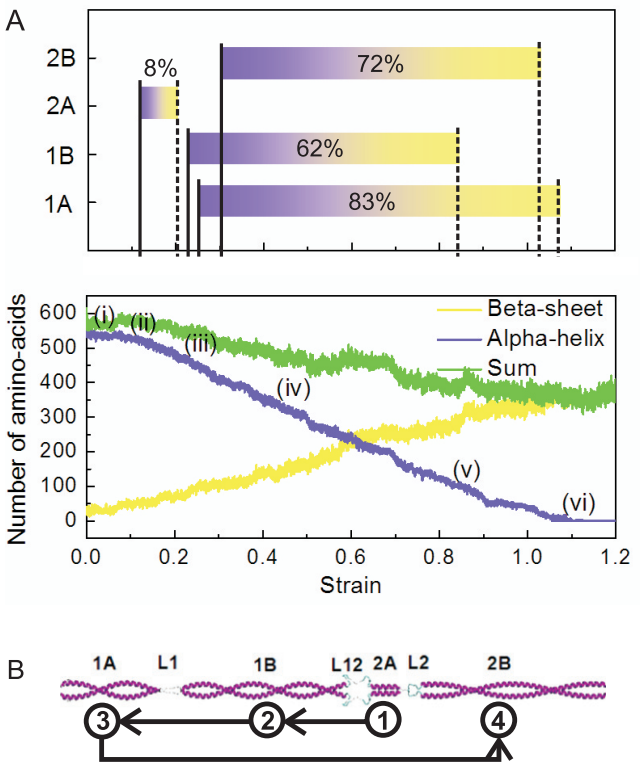

Figure 6. Geometry–strain maps for the dimer as it undergoes tensile deformation. Panel A: the lower part of the plots shows the number of amino acids associated with alpha-helical structure (purple) or beta-sheet structure (yellow), and the sum for these two known structures (green). The bars shown in the upper part of the plot denote processes of α–β transition for each segment. Each point marked corresponds to a snapshot with the same label shown in figure 4. The strain values in the upper part of the plot indicate the strain amount required to complete unfolding of the particular domain, with the 2A domain requiring the smallest amount of strain (8%) and the 1A domain requiring the largest amount of strain (83%). Panel B: schematic of unfolding sequence of domains 1A, 1B, 2A and 2B.

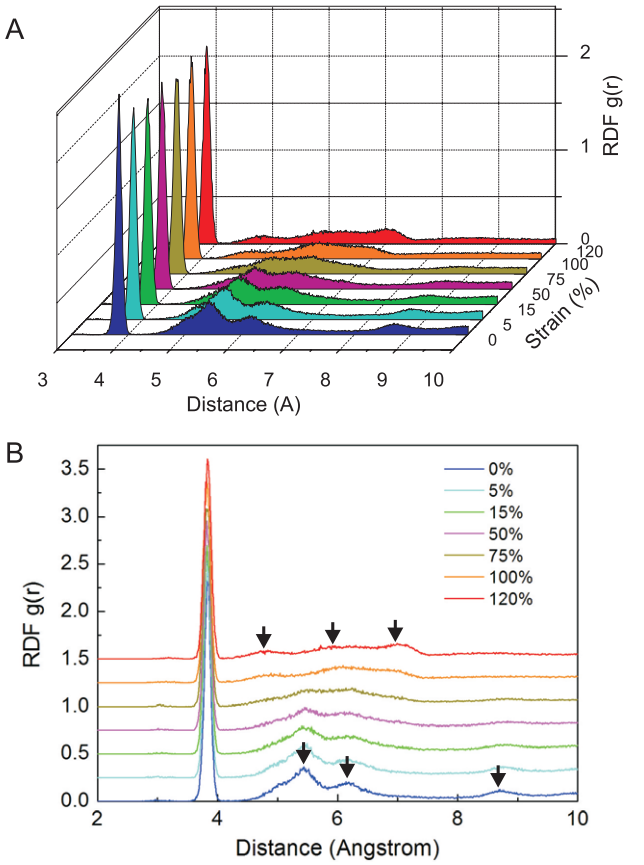

Figure 7. Radial distribution function (RDF) analysis for the dimer structure at pulling strain varies from 0 to 120% (panel A: three-dimensional view; panel B: two-dimensional view, where the curves corresponding to different strains are shifted by 0.25 for better visualization). The first peak at 3.84 Å is for the character of first-order structure. The other peaks for 5.00, 5.46, 6.20 and 8.70 Å gives the first, second, third and fourth neighborhood within the secondary and third structures of the dimer protein. During increasing strain, the higher-order peaks (rather than the first peak associated with the polypeptide backbone) becomes less pronounced and broader, showing the character of structural change as the protein undergoes tensile deformation.

$x_b = 4.27$ Å. For the fast deformation regime, we obtain $E_b = 5.18$ kcal mol^{-1} and $x_b = 0.64$ Å. It is noted that the energy barrier and distance of the transition point for slow deformation are much larger than for fast deformation, indicating that fewer H-bonds rupture simultaneously in the fast deformation mode than in the slow deformation mode, in agreement with earlier results reported in [15] (albeit these simulations were carried out in a single alpha-helix protein domain). The results of the energy landscape parameters are summarized in table 2 and visualized in figure 8(C). In earlier studies [25] it has been suggested that the protein structure strength increases as a weak power of rate under slow loading. Based on this suggestion, we use an overall fitting function to the data defined as

$$f_{\text{fit}}(v) = A \exp\left(\frac{\ln(v)}{B}\right), \tag{1}$$

which empirically captures the asymptotic trend of the strength properties for a very wide variation of pulling speeds (where v is expressed in SI units in equation (1)). The parameters $A = 222.77$ pN and $B = 6.634$ are obtained by fitting equation (1) to the overall simulation results as shown in figure 8(A). The prediction of equation (1) for pulling velocities comparable to those used in experiment (of the order of 8×10^{-12} Å ps^{-1}) is ≈10 pN, in agreement with experimental results [20] that reported a strength of 15.7 pN in regime (II). For the coiled-coil myosin structure, the unfolding force measured by atomic force microscopy (with a cantilever speed of 1 μm s^{-1}) is ≈33 pN [18], while from our model the unfolding force for this pulling velocity is found to be 28 pN. This comparison suggests a rather good agreement with experimental results. It is noted that the force at the angular point is significant as it provides an estimate of the force plateau seen in regime (II) (see figure 3(A), with an increase of the force during deformation as discussed above). Thus equation (1) could also be used in the development of coarse-grained or micromechanical models.

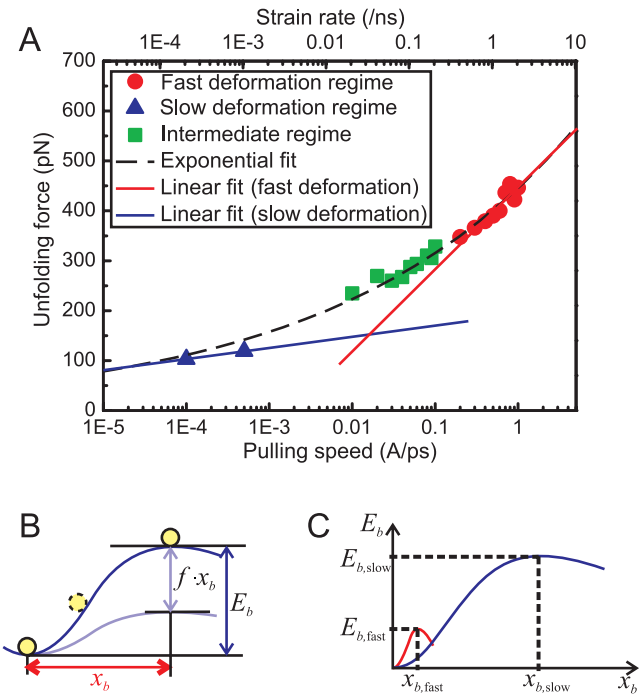

Figure 8. Unfolding force at the angular point varying with the pulling speed and corresponding strain rate, and schematic of the energy landscape. Panel A: each point refers to a simulation with a specific pulling velocity. As the speed increases, the strength increases. The blue line is a linear fit to the slow deformation regime, while the red line is a fit to the fast deformation regime. The green points refer to the intermediate regime. The dashed black curve is an overall exponential fit to the data. Panel B: schematic of the energy landscape, illustrating the meaning of the parameters x_b and E_b (see table 2 for a summary of the resulting energy landscape parameters). Panel C: change of the energy landscape from the fast to the slow deformation regime. The changes in x_b and E_b reflect the simulation results shown in table 2.

3. Discussion

We have utilized an atomistic model of human vimentin dimer and carried out molecular dynamics simulations to measure its response to mechanical stress, under tensile loading. To the best of our knowledge, this is the first nanomechanical analysis of the vimentin dimer at atomistic resolution. Our analysis provides detailed insight into molecular-level deformation mechanisms and enabled us to link the force–strain behavior (figure 3(A)) to geometric changes in the structural make-up of the protein at different hierarchical levels (figures 4–7). The most salient feature of intermediate filaments is that the filament is rather compliant at low strain, whereas it becomes much stiffer at high strain, as confirmed in the analysis shown in figure 3(A) (see also tangent fits to the slope in regimes I, II and III). We find that large deformation of the dimer is accompanied by an α–β transition, a phenomenon that has been observed for other long alpha-helical coiled-coil protein filaments such as α-keratin intermediate filament fibers [14, 21, 22, 26] and intermediate filament hagfish slime threads [7, 20]. Our simulations reveal that the deformation process is associated with a particular pattern of domain unfolding, as shown in figure 6 and table 1. This could play an important role in biomechanical signaling pathways, where specific levels of strain may correspond to particular changes in the molecular structure. Thereby the unfolding of specific domains might induce biochemical signaling, which may be part of the coupling between deformation state and biological processes. The results depicted in figure 8(A) show that the unfolding force of the dimer structure depends strongly on the pulling speed, with average rupture forces in the range of 10–600 pN in regime (II). The overall fit provided in equation (1) represents a general formula to express the strength for varying pulling velocities.

Table 2. Energy landscape parameters x_b and E_b, extracted using the Bell model, for pulling simulations of the dimer with different deformation modes (as a function of pulling speed v). See figure 8(B) for a schematic of the energy landscape and associated parameters and figure 8(C) for a visualization of the two regimes presented here.

Energy landscape parameters	Slow regime ($v < 0.001$ Å ps^{-1})	Fast regime ($v > 0.2$ Å ps^{-1})
x_b (Å)	4.27	0.64
E_b (kcal mol^{-1})	14.05	5.18

The analysis reported here provides a new way forward in carrying out molecular-level studies of intermediate filament structure–property relationships. For example, the approach allows for the possibility of probing the effect of mutations using *in silico* materiomics. This could enable pathogenesis studies of severe medical conditions associated with genetic mutations in intermediate filaments. The emerging significance of intermediate filaments in many cellular processes suggests that the results of our study may also contribute to develop an improved understanding of cell mechanical properties, specifically deformation, cell adhesion and mechanotransduction. Intermediate filaments can also be considered as a model system that may enable us to fabricate *de novo* engineered materials that display a high sensitivity to applied forces, show resilient mechanical properties and provide biological compatibility, perhaps by generating hierarchical structures as discussed in [8]. This could facilitate the design of a new class of materials with applications as self-assembled nanomaterials, biomaterials, stimulus responsive gels or perhaps as energy absorbing structural materials.

4. Materials and methods

4.1. Molecular models and force fields

Molecular dynamics simulations are carried out using the CHARMM program by using the CHARMM19 all-atom energy function with an effective Gaussian model for the water solvent [27, 28]. This molecular model is currently the only feasible approach to simulate sufficiently large protein structures at long timescales (reaching 70 ns for 0.01 Å ps^{-1} and 170 ns for 0.0001 Å ps^{-1} pulling speed), and is thus used for structure prediction and mechanical characterization. Furthermore, the use of the effective solvent model is motivated by our desire to overcome the limitations of relatively fast unfolding rates used in the simulations. The

lack of slow water relaxation processes in the implicit model enables us to effectively model the physical conditions of pulling experiments at much longer timescales. Therefore, effective solvent methods provide physically more meaningful results than the use of explicit solvent methods, as discussed in [29]. Due to the size of the protein, the simulations reported here take up to 50 days each on a parallel Linux cluster (30 days for 0.01 Å ps^{-1} and 50 days for 0.0001 Å ps^{-1}). The molecular model used here is based on the structure reported in [30], developed based on the amino acid sequence and experimental structural data.

4.2. Nanomechanical characterization

The C^{α} atoms at the end of two 2B segments are pulled on by using steered molecular dynamics (SMD), while the other end of the filament is fixed (with a force constant of 10 kcal mol^{-1} $Å^{-2}$). The pulling force F is recorded versus the position. The simulations are carried out at pulling velocities ranging from 0.0001 to 1 Å ps^{-1}. The analysis of the mechanical properties is facilitated by calculating engineering stress and strain. We record the force–displacement curve from steered molecular dynamics simulation and analyze the mechanical properties by computing the engineering strain, which is defined as

$$\varepsilon = \Delta L/L_0, \tag{2}$$

where ΔL, and L_0 are the displacement, and initial length, respectively. The engineering stress is defined as

$$\sigma = F/A_0, \tag{3}$$

where F and A_0 are pulling force and relevant cross-sectional area. The (tangent) Young's modulus is determined by

$$E = \frac{\Delta\sigma}{\Delta\varepsilon}. \tag{4}$$

The average diameter of the cross section of the dimer is $d_{\text{dimer}} \approx 2$ nm. The value of A_0 is calculated by assuming a circular cross section of the protein.

4.3. Dependence of mechanical properties on pulling speed

To obtain information about the pulling-speed-dependent behavior, we carry out SMD simulations with varying pulling rates. The Bell model is used to theoretically describe the characteristics of the force–speed curve and to extract energy landscape parameters [31] (see figure 8(B) for a schematic of the energy landscape and definition of variables). In this model, the unfolding force has an explicit relation with the pulling speed as given in [15]:

$$f = \frac{k_B T}{x_b}\ln(v) - \frac{k_B T}{x_b}\ln(v_0), \tag{5}$$

where k_B is Boltzmann's constant, T is the temperature, x_b is the distance that needs to be overcome to break an H-bond, v is the pulling speed and v_0 is the natural bond-breaking speed defined as

$$v_0 = \omega_0 x_b \exp\left(-\frac{E_b}{k_B T}\right). \tag{6}$$

Here $\omega_0 = 1 \times 10^{13}$ s^{-1} is the natural vibration frequency and E_b is the energy barrier during unfolding (it is noted we use SI units to deduce the functions and parameters).

4.4. Molecular structure analysis

We use the visual molecular dynamics (VMD) program [32] for visualization of protein structures as well for the analysis of the α–β transition shown in figure 6, using the approach suggested in [33]. The rupture length of H-bonds is 3.7 Å for visualization in VMD. The RDF functions are calculated using the 'gofr' plug-in of VMD. The criterion to identify H-bonding considers both hydrogen bond patterns and the backbone geometry generally expressed as polypeptide chain dihedral angles.

Acknowledgment

We acknowledge support by the Air Force Office of Scientific Research (grant no. FA9550-08-1-0321).

References

[1] Alberts B *et al* 2002 *Molecular Biology of the Cell* (New York: Taylor and Francis)
[2] Herrmann H and Aebi U 2004 Intermediate filaments: molecular structure, assembly mechanism, and integration into functionally distinct intracellular scaffolds *Annu. Rev. Biochem.* **73** 749–89
[3] Hutchison C J 2002 Lamins: building blocks or regulators of gene expression? *Nat. Rev. Mol. Cell Biol.* **3** 848–58
[4] Herrmann H *et al* 2007 Intermediate filaments: from cell architecture to nanomechanics *Nat. Rev. Mol. Cell Biol.* **8** 562–73
[5] Wang N, Butler J P and Ingber D E 1993 Mechanotransduction across the cell surface and through the cytoskeleton *Science* **260** 1124–7
[6] Wang N and Stamenovic D 2002 Mechanics of vimentin intermediate filaments *J. Muscle Res. Cell Motil.* **23** 535–40
[7] Fudge D *et al* 2008 The intermediate filament network in cultured human keratinocytes is remarkably extensible and resilient *PLoS ONE* **3** e2327
[8] Ackbarow T *et al* 2009 Alpha-helical protein networks are self protective and flaw tolerant *PLoS ONE* **4** e6015
[9] Lewis M K *et al* 2003 Concentric intermediate filament lattice links to specialized Z-band junctional complexes in sonic muscle fibers of the type I male midshipman fish *J. Struct. Biol.* **143** 56–71
[10] Kreplak L, Herrmann H and Aebi U 2008 Tensile properties of single desmin intermediate filaments *Biophys. J.* **94** 2790–9
[11] Ackbarow T and M J Buehler 2007 Superelasticity, energy dissipation and strain hardening of vimentin coiled-coil intermediate filaments: atomistic and continuum studies *J. Mater. Sci.* **42** 8771–87
[12] Zhang H, Ackbarow T and Buehler M J 2008 Muscle dystrophy single point mutation in the 2B segment of lamin A does not affect the mechanical properties at the dimer level *J. Biomech.* **41** 1295–301
[13] Kreplak L and Bar H 2009 Severe myopathy mutations modify the nanomechanics of desmin intermediate filaments *J. Mol. Biol.* **385** 1043–51
[14] Kreplak L, Doucet J and Briki F 2001 Unraveling double stranded alpha-helical coiled coils: an x-ray diffraction study on hard alpha-keratin fibers. *Biopolymers* **58** 526–33
[15] Ackbarow T *et al* 2007 Hierarchies, multiple energy barriers, and robustness govern the fracture mechanics of alpha-

helical and beta-sheet protein domains *Proc. Natl Acad. Sci. USA* **104** 16410–5
[16] Schwaiger I *et al* 2002 The myosin coiled-coil is a truly elastic protein structure *Nat. Mater.* **1** 232–5
[17] Bertaud J, Qin Z and Buehler M J 2009 Atomistically informed mesoscale model of alpha-helical protein domains *Int. J. Multiscale Comput. Eng.* **7** 237–50
[18] Root D D *et al* 2006 Coiled-coil nanomechanics and uncoiling and unfolding of the superhelix and alpha-helices of myosin *Biophys. J.* **90** 2852–66
[19] Guzman C *et al* 2006 Exploring the mechanical properties of single vimentin intermediate filaments by atomic force microscopy *J. Mol. Biol.* **360** 623–30
[20] Fudge D S *et al* 2003 The mechanical properties of hydrated intermediate filaments: insights from hagfish slime threads *Biophys. J.* **85** 2015–20
[21] Kreplak L *et al* 2004 New aspects of the alpha-helix to beta-sheet transition in stretched hard alpha-keratin fibers *Biophys. J.* **87** 640–7
[22] Kreplak L and Fudge D 2007 Biomechanical properties of intermediate filaments: from tissues to single filaments and back *Bioessays* **29** 26–35
[23] Parry D A D 2006 Hendecad repeat in segment 2A and linker L2 of intermediate filament chains implies the possibility of a right-handed coiled-coil structure *J. Struct. Biol.* **155** 370–4
[24] Parry D A D *et al* 2007 Towards a molecular description of intermediate filament structure and assembly *Exp. Cell Res.* **313** 2204–16
[25] Evans E and Ritchie K 1997 Dynamic strength of molecular adhesion bonds *Biophys. J.* **72** 1541–55
[26] Hearle J W S 2000 A critical review of the structural mechanics of wool and hair fibres *Int. J. Biol. Macromol.* **27** 123–38
[27] Lazaridis T and Karplus M 1997 'New view' of protein folding reconciled with the old through multiple unfolding simulations *Science* **278** 1928–31
[28] Lazaridis T and Karplus M 1999 Effective energy function for proteins in solution *Proteins—Struct. Funct. Genet.* **35** 133–52
[29] Paci E and Karplus M 2000 Unfolding proteins by external forces and temperature: the importance of topology and energetics *Proc. Natl Acad. Sci. USA* **97** 6521–6
[30] Qin Z, Kreplak L and Buehler M J 2009 Hierarchical structure controls nanomechanical properties of vimentin intermediate filaments *PLoS ONE* at press doi:10.1371/journal.pone.000729
[31] Bell G I 1978 Models for specific adhesion of cells to cells *Science* **200** 618–27
[32] Humphrey W, Dalke A and Schulten K 1996 VMD: visual molecular dynamics *J. Mol. Graph.* **14** 33
[33] Frishman D and Argos P 1995 Knowledge-based protein secondary structure assignment *Proteins—Struct. Funct. Genet.* **23** 566–79